Void Fraction and Interfacial Friction in Vertical Circular Pipes with the Square Top End Under Flooding Conditions

Takaki, Toshiya
Murase, Michio
Hayashi, Kosuke
Tomiyama, Akio

(Citation)
Nuclear Technology,208(3):503-519

(Issue Date)
2021-10-19

(Resource Type)
journal article

(Version)
Accepted Manuscript

Void Fraction and Interfacial Friction in Vertical Circular Pipes with the Square Top End under Flooding Conditions

Toshiya Takaki,[a,b]* Michio Murase,[a] Kosuke Hayashi,[b] and Akio Tomiyama[b]

[a] *Institute of Nuclear Safety System, Inc., 64 Sata, Mihama-cho, Mikata-gun, Fukui 919-1205, Japan*

[b] *Kobe University, 1-1 Rokkodai, Nada-ku, Kobe-shi, Hyogo 657-8501, Japan*

* takaki.toshiya@inss.co.jp

Keywords: *Flooding, interfacial friction factor, liquid film thickness, square top end, vertical pipe*.

Pages of Text: 24

Number of Table: 1

Number of Figures: 19

Abstract

The objective of this study was to reduce the uncertainties of correlations for flow characteristics in vertical pipes under flooding at the top end. The void fraction α, pressure gradient dP/dz, and countercurrent flow limitation (CCFL) were previously measured with diameter D = 40 mm and working fluid of air and water. The wall friction and interfacial friction factors (f_w and f_i) were obtained based on the annular flow model, and CCFL and f_w were evaluated in detail. Hence evaluations of α and f_i were turned out attention in detail. The liquid film thickness δ and f_i for the smooth film (SF) due to flooding at the top end were obtained by using the previously derived f_w correlation and existing dP/dz data with D = 20-50.8 mm and pressure P = 0.1-4.1 MPa, and empirical correlations for δ and f_i were derived. δ was well expressed by a function of the liquid Reynolds number Re_L, and the uncertainty of the δ correlation was ±0.0062 for α = 0.87-0.98. f_i was expressed by a function of δ/L (where L is the Laplace length) or the Kutateladze parameter K_G^*, the dimensionless diameter D^* (= D/L), and the density ratio of gas and liquid phases ρ_G/ρ_L. The applicability of the derived correlations to conditions of D = 300 mm and P = 7 MPa was evaluated, and the f_i correlation was modified based on f_i values computed with the δ correlation. The drift-flux parameters for SF were also considered.

I. INTRODUCTION

In an accident analysis for light water reactors such as a pressurized water reactor (PWR) and a boiling water reactor (BWR), models and correlations for flow characteristics under flooding conditions are important to evaluate the pressure loss and the distribution of the coolant mass in the system. The objective of this study was to reduce uncertainty of correlations for countercurrent flow limitation (CCFL), the void fraction α, the wall friction factor f_w, and the interfacial friction factor f_i under flooding conditions, which are used in an accident analysis. While many flooding studies have been done,[1,2] flow characteristics in vertical pipes under flooding conditions depend on the top and bottom end shapes, and the characteristics are not well understood mainly due to lack of data for α. Bharathan et al.[3] measured CCFL (i.e. relationship between the time-averaged superficial gas and liquid velocities J_G and J_L), pressure gradient dP/dz, and the liquid film thickness δ in vertical pipes, and obtained f_w and f_i under flooding conditions based on the annular flow model. They classified the liquid film as the rough film (RF) due to flooding at the bottom end and as the smooth film (SF) due to flooding at the top end. δ was under-detected for large δ and the obtained f_w was sometimes negative. Subsequently, Bharathan et al.[4] and Bharathan and Wallis[5] obtained f_i from the measured dP/dz by assuming $f_w = 0$, and proposed an f_i correlation for RF. However, they offered little discussion on SF. Figure 1 illustrates the top and bottom end shapes in a vertical pipe and the flow patterns under flooding conditions. The flow patterns depend on the relationship between the falling liquid flow rates limited by flooding at the top and bottom ends $W_{L,T}$ and $W_{L,B}$. The bottom end shape of the heat transfer tubes in a steam generator is square, and the top end shape of the pressurizer surge line is square.

In our research group, Goda et al.[6] measured CCFL, dP/dz and α by using quick closing valves in vertical pipes (diameter of D = 20 and 40 mm; the rounded top end and square (i.e. sharp-edged without curvature) bottom end; working fluid of air and water), and obtained f_w and f_i. Shimamura et al.[7] and Takaki et al.[8] carried out similar experiments to Goda et al.[6] with the square top end and rounded bottom end, and working fluid of air and water for D = 20 mm and 40 mm, respectively, and they obtained f_w and f_i. Table I lists their experimental conditions[6,7,8] in comparison with those by Bharathan et al.[3] and Ilyukhin et al.[9] Bharathan et al.[3] measured δ but uncertainty for the measurement was large. Ilyukhin et al.[9] did not measure α but measured dP/dz. Takaki et al.[8] previously evaluated CCFL characteristics and f_w for SF in detail, because they are important to obtain α and f_i from the dP/dz data. However, evaluation of α (or δ) and f_i remained to be an unresolved subject.

The objective of this paper was to obtain α and f_i for SF flooding at the square top end by using the f_w correlation proposed by Takaki et al.[8] and existing dP/dz data and to derive their correlations, which can be used in an accident analysis up to 7 MPa steam-water conditions. To evaluate features of flow characteristics for RF and SF, we firstly compared the data by Goda et al.[6] for $D = 40$ mm with the square bottom end and the data by Takaki et al.[8] for $D = 40$ mm with the square top end. Then, we obtained α and f_i from dP/dz data reported by Bharathan et al.[3] and Ilyukhin et al.,[9] and we derived empirical correlations for δ and f_i for SF by using data listed in Table I. The water level h in the upper tank affects CCFL characteristics.[10,11] Bharathan et al.[3] classified h to $h > 2D$ and $h < D$, and we used data with $h > 2D$. Ilyukhin et al.[9] did not report the h values, and we judged that h was high from the experimental setup drawing. Takaki et al.[12] showed that α and f_i could be accurately obtained from the dP/dz data and a reliable f_w correlation by using the annular flow model. We also examined the drift-flux parameters (Zuber and Findlay[13]) for SF, because the drift flux model is used in some accident analysis codes. We finally evaluated applicability of the derived correlations to large diameter ($D = 0.3$ m which is the diameter of the pressurizer surge line in a PWR) and high pressure ($P = 7$ MPa) steam-water conditions.

II. EVALUATION METHOD AND FLOW CHARACTERISTICS UNDER FLOODING CONDITIONS

II.A. Annular Flow Model and Flow Patterns

In the annular flow model, the force balance equations for the gas core and the entire cross section are expressed in dimensionless forms as:[5,6,8,12]

$$\left(\frac{dP}{dz}\right)^{*} + \frac{\rho_G}{\rho_L - \rho_G} + \left(\frac{2f_i}{\alpha^{1/2}}\right)\left\{\frac{J_G^{*}}{\alpha} - \left(\frac{\rho_G}{\rho_L}\right)^{1/2}\frac{J_L^{*}}{1-\alpha}\right\}^{2} = 0\,, \tag{1}$$

and

$$\left(\frac{dP}{dz}\right)^{*} + \left\{(1-\alpha) + \frac{\rho_G}{\rho_L - \rho_G}\right\} - 2f_w\left(\frac{J_L^{*}}{1-\alpha}\right)^{2} = 0\,, \tag{2}$$

where

$$J_i^{*} = \frac{J_i}{\left[\{gD(\rho_L - \rho_G)\}/\rho_i\right]^{1/2}} \qquad (i = G \text{ or } L) \tag{3}$$

and

$$\left(\frac{dP}{dz}\right)^{*} = \frac{dP/dz}{(\rho_L - \rho_G)g}\;. \tag{4}$$

Additionally, here D is the diameter, f_i is the interfacial friction factor, f_w is the wall friction factor, g is the gravitational acceleration, J is the superficial velocity, J^* is the Wallis parameter, P is the pressure, z is the vertical coordinate, α is the void fraction, and ρ is the density. The subscripts G and L denote the gas and liquid phases, respectively. $J_G > 0$ for the upward flow of the gas phase, while $J_L < 0$ for falling liquid motion. We can obtain f_i and f_w from Eqs. (1) and (2), respectively, by measuring CCFL (J_L for a given J_G), dP/dz, and α.

Figure 2 (a) shows flow characteristics (the liquid volume fraction $(1-\alpha)$, $|dP/dz|^*$

and J_L^*) in a vertical pipe with D = 20 mm, and the square top and rounded bottom ends under flooding conditions reported by Shimamura et al.[7] All flow patterns of SF, TR (transition from SF to RF) and RF appeared in the experiments. Figure 2 (b) shows the time-strip images,[7] where the gray values of pixels along the pipe axis were extracted from each image taken by using a high-speed video camera with the frame rate of 350 fps and were rearranged in the horizontal direction. In the region of J_G < 5.9 m/s, J_L was limited at the top end as shown in Fig. 1 (b) and the relatively smooth film (SF) formed in the vertical pipe. However, the downward motion of interfacial waves were observed even in SF due to intermittent liquid inflow at the top end. In the region of 5.9 m/s < J_G < 7.4 m/s (where the flow pattern was TR), the disturbance waves appeared due to flooding near the bottom end, and J_L was limited at the top and bottom ends simultaneously (see Fig. 1 (b)). The disturbance waves did not reach to the upper tank. In the region of J_G > 7.4 m/s, the disturbance waves flew up to the upper tank in RF. $(1-\alpha)$ decreases with increasing J_G in SF and RF but increases with increasing J_G in TR depending on the heights of regions for RF and SF (see Fig. 1 (b) and Fig. 2 (b)). In Eqs. (1) and (2), $\rho_G/(\rho_L-\rho_G) << 1$. Hence $|dP/dz|^*$ is nearly equal to the f_i term or the difference between $(1-\alpha)$ and the f_w term.

The diameter and shapes at the top and bottom ends affected J_G at the flow pattern transition.[6,8] In the vertical pipe with D = 20 mm, and the rounded top and square bottom ends (R/S),[6] the disturbance waves at the bottom end occurred at low J_G, and the flow pattern was RF in the region of J_G > 2.5 m/s. This was because flooding at the square bottom end occurred at low J_G.

II.B. CCFL Characteristics

The Wallis CCFL correlation[1] defined by Eq. (5) is widely used in accident analysis codes to compute J_L for a given J_G under flooding conditions.

$$J_G^{*1/2} + m\,|J_L|^{*1/2} = C, \tag{5}$$

where C and m are empirical constants. Kusunoki et al.[14] proposed Eq. (6) for flooding at the bottom end.

$$\frac{J_G^{*1/2}}{(\mu_G/\mu_L)^{0.07}} = (1.04 \pm 0.05) - 3.6\left\{\left(\frac{\mu_G}{\mu_L}\right)^{0.1}|J_L|^{*1/2}\right\} + 11\left\{\left(\frac{\mu_G}{\mu_L}\right)^{0.1}|J_L|^{*1/2}\right\}^2$$
$$-16\left\{\left(\frac{\mu_G}{\mu_L}\right)^{0.1}|J_L|^{*1/2}\right\}^3 \qquad (14\text{ mm} \le D \le 51\text{ mm}) \tag{6}$$

Eq. (6) was modified to the Wallis correlation (i.e. a linear function of $J_G^{*1/2}$ and $|J_L|^{*1/2}$) for an accident analysis,[15] but its uncertainty was large due to the effect of fluid properties. Murase et al.[11] proposed Eq. (7) with the Kutateladze parameters K_i^* for flooding at the top end.

$$K_G^{*1/2} + 0.97\,|K_L|^{*1/2} = 1.53 \pm 0.11 \quad (11 \le D^* \le 94), \tag{7}$$

where

$$K_i^* = D^{*1/2} J_i^*$$
$$= \frac{J_i}{\{\sigma g(\rho_L - \rho_G)/\rho_i^2\}^{1/4}} \qquad (i = G \text{ or } L) \tag{8}$$

$$D^* = \frac{D}{L}, \tag{9}$$

$$L = \left\{\frac{\sigma}{(\rho_L - \rho_G)g}\right\}^{1/2}, \tag{10}$$

where L is the Laplace length and σ is the surface tension.

Figure 3 shows CCFL characteristics with D = 40 mm, and the square top and rounded bottom ends (S/R)[8] and the rounded top and square bottom ends (R/S).[6] In both cases, flooding occurred near the top end and falling liquid formed SF in the region of low J_G; with increasing J_G, the SF was further changed in the transition region (TR: where flooding occurred near the top and bottom ends simultaneously). J_L was larger for R/S than for S/R due to the rounded top end for SF, but J_L became similar in both cases for the TR even though there was a different shape at the bottom end. $C_W = (1.04\pm0.05)(\mu_G/\mu_L)^{0.07} = 0.79\pm0.038$ for air-water in Eq. (6) and $C_W = (1.53\pm0.11)/D^{*1/4} = 0.78\pm0.056$ for D = 40 mm in Eq. (7). The difference between values obtained by Eqs. (6) and (7) was small. J_L^* measured with S/R agreed well with Eq. (6) for R/S except in the region of small J_G^*. J_L^* for S/R was lower than the mean value of Eq. (7) for S/R in the region of large J_G, but was within the uncertainty of ± 0.11 in Eq. (7).

The slope m in Eq. (5) was larger for S/R except in the region of large J_G^* than for R/S, and this was the cause of flooding near the top end at low J_G^* and near the bottom end at medium to larger J_G^*. The transition point from SF to TR may be given by the intersection of CCFL curves near the top end and near the bottom end.

II.C. Void Fraction and Pressure Gradient

Figure 4 shows $(1-\alpha)$ and $-(dP/dz)^*$ defined by Eq. (4) for S/R[8] and R/S.[6] The difference between $(1-\alpha)$ and $-(dP/dz)^*$, i.e. $(1-\alpha)+(dP/dz)^*$, nearly equals the f_w term, because $\rho_G/(\rho_L-\rho_G)$ is very small in Eq. (2). At the largest J_G for S/R, the occurrence of TR or RF was not clear from a visual observation. $(1-\alpha)$ and $-(dP/dz)^*$ differed between S/R and R/S due to the different flow structure. The f_w term was large for SF and small for RF. Bharathan and Wallis[5] neglected the f_w term for RF. They indicated that the f_w term for SF cannot be neglected, but they did not propose a correlation for f_w in SF. For S/R, the TR region was broad. SF, TR and RF are for classification of flow structure shown by Bharathan and Wallis,[5] and the gas-liquid interface in SF is not actually smooth due to interfacial waves caused by intermittent liquid inflow at the top end (see Fig. 2

(b)).[8]

Even for SF at small J_G^*, $(1–\alpha)$ and $–(dP/dz)^*$ were larger for R/S than those for S/R due to the larger J_L (see Fig. 3). In the region of large J_G^* (> 0.5), $(1–\alpha)$ and $–(dP/dz)^*$ were larger for S/R than they were for R/S, and the reason of this was not clear. In the region of medium J_G^*, where it was larger than J_G^* at the transition point from SF to TR for S/R ($J_G^* = 0.26$, $J_G = 4.7$ m/s), J_L^* was almost the same between S/R and R/S as shown in Fig. 3, but $(1–\alpha)$ and $–(dP/dz)^*$ were much smaller for S/R than they were for R/S due to the differences of the shape of the bottom end (square or rounded) and formation of disturbance waves there.

It is well known that J_L^* is the largest with the rounded top and bottom ends (R/R) among combinations of the top and bottom end shapes shown in Fig. 1 (a),[1,2] but reliable α data in vertical pipes with R/R are not found. Measurement of α with R/R is remains as future work.

II.D. Wall Friction Factor

$(dP/dz)^*$ and α data are needed to obtain f_w from Eq. (2), but α data under flooding conditions are limited. Therefore, f_w for single-phase flows is widely used,[12,16] and the f_w correlation is expressed by:

$$f_w = \max\left(\frac{16}{Re_L} \ , \ \frac{0.079}{Re_L^{0.25}} \right) \ , \tag{11}$$

$$Re_L = \frac{|J_L| D}{\nu_L}, \tag{12}$$

where Re_L is the liquid Reynolds number and ν is the kinematic viscosity. Takaki et al.[8] proposed a f_w correlation ($f_w = 0.70/Re_L^{0.50}$) for the transition region between laminar and turbulent flows, and they speculated that the correlation could be combined with Eq. (11), i.e.:

$$f_w = \max\left(\frac{16}{Re_L}\ ,\ \frac{0.70}{Re_L^{\ 0.50}}\ ,\ \frac{0.079}{Re_L^{\ 0.25}}\right)\ . \tag{13}$$

Figure 5 shows f_w for S/R[8] and R/S[6] as a function of Re_L. f_w was obtained from Eq. (2) by using the measured CCFL (J_L for given J_G), dP/dz, and α. f_w for SF was expressed well by Eq. (13). In the laminar flows for D = 40 mm, f_w for both S/R and R/S was well expressed by the correlation proposed by Goda et al.:[6]

$$f_w = \frac{28600}{Re_L^{\ 1.96}}\ . \tag{14}$$

The liquid downward and upward flows due to the flooding near the bottom end and formation of disturbance waves in TR and RF increased the velocity gradient near the wall, and this increased f_w. Figure 5 suggested that the liquid velocity distribution near the wall would be similar between TR for S/R and RF for R/S in D = 40 mm.

II.E. Interfacial Friction Factor

The f_i can be computed by using Eq. (1), empirical correlations for J_L and f_w (Eqs. (7) and (13) for SF for example), and a correlation for α. However, a correlation for f_i is sometimes used in accident analysis codes. Bharathan and Wallis[5] proposed a correlation for f_i derived from dP/dz data for RF reported by Bharathan et al.:[4]

$$f_i = 0.005 + A\left(\frac{\delta}{L}\right)^{\mathrm{B}}\ ,$$

$$\log_{10} A = -0.56 + \frac{9.07}{D^*}\ ,$$

$$B = 1.63 + \frac{4.74}{D^*}\ . \tag{15}$$

Sano et al.[17] proposed an f_i correlation for RF by using previously reported data.[4,6] The f_i correlation for air-water conditions was expressed by:

$$f_i = 0.30D^* \exp(-1.90K_G^*). \tag{16}$$

The form of Eq. (16) is simple in comparison with Eq. (15). Both Eqs. (15) and (16) are for RF. On the other hand, a suitable f_i correlation for SF has not been proposed.

Figure 6 shows f_i for S/R[8] and R/S.[6] f_i was obtained from Eq. (1) by using the measured CCFL (J_L for given J_G), dP/dz, and α. f_i differed between S/R and R/S due to the different $(1-\alpha)$ (see Fig. 4). Eqs. (15) and (16) were derived for RF, but Eq. (15) underestimated f_i except for the region of large J_G. In TR of S/R, f_i increased and decreased with increasing J_G (we expected a narrow region for TR and simple increase of f_i with increasing J_G). The reason for this complex change in f_i was not clear, but might be due to unstable generation of disturbance waves near the rounded bottom end. The f_i value at large J_G was larger for S/R than that for R/S (we expected RF occurrence and similar f_i values for S/R and R/S at large J_G).

III. LIQUID FILM THICKNESS AND INTERFACIAL FRICTION FOR SMOOTH FILM

Takaki et al.[8] evaluated CCFL characteristics and f_w for SF due to flooding at the top end in detail, but did not discuss α (or δ) and f_i in detail. In this section, therefore, we obtained δ and f_i by using the f_w correlation reported by Takaki et al.[8] and dP/dz data reported by Bharathan et al.[3] and Ilyukhin et al.,[9] and we discussed δ and f_i for SF in detail.

III.A. Liquid Film Thickness

The relationship between α and δ in the annular flow can be expressed by:

$$\alpha = \left(1 - \frac{2\delta}{D}\right)^2 \quad \text{or} \quad \frac{\delta}{D} = \frac{1 - \alpha^{1/2}}{2} . \tag{17}$$

Kamei et al.[18] were the first to measure δ with the weighting method under flooding conditions, and they showed δ under flooding conditions was thicker than δ for the free falling film. However, uncertainty of their measurements was large. Feind[19] and Hewitt and Wallis[20] measured δ under countercurrent flow conditions just before the onset of flooding or formation of laminar liquid films and found δ under countercurrent flow conditions was similar to δ for the free falling film. Therefore, Nusselt's equation[21] for laminar flows in free falling films is widely used for δ in SF. Imura et al.[22] used Feind's experimental equation[19] for turbulent flows to compute α under flooding conditions. The combination of Nusselt's equation and Feind's experimental equation is given by:

$$\frac{\delta}{L_v} = \max\left\{ \left(\frac{3Re_L}{4}\right)^{1/3} \ , \ 0.266 {Re_L}^{1/2} \right\} , \tag{18}$$

$$L_v = \left(\frac{{v_L}^2}{g}\right)^{1/3} . \tag{19}$$

Takaki et al.[12] obtained α by using Eq. (2), a correlation for f_w, and the $(dP/dz)^*$ and CCFL data by Bharathan et al.[3] with D = 50.8 mm and air-water and by Ilyukhin et al.[9] with D = 20 mm and steam-water at P = 0.6-4.1 MPa, and they proposed a δ correlation for turbulent flows. The correlation for turbulent flows in Eq. (18) was replaced as:

$$\frac{\delta}{L_v} = \max\left\{ \left(\frac{3Re_L}{4}\right)^{1/3} \ , \ 0.091 {Re_L}^{0.64} \right\} . \tag{20}$$

Figure 7 shows δ/L_v for S/R[8] and R/S[6] with D = 40 mm. For a J_G^* value, $(1-\alpha)$ for SF was larger for R/S than that for S/R as shown in Fig. 4, but the relationship between δ/L_v and Re_L for SF was close between S/R and R/S as shown in Fig. 7 because J_L^* (i.e.

Re_L) for SF was larger for R/S than that for S/R as shown in Fig. 3. The δ/L_v data by Shimamura et al.[7] with D = 20 mm are shown only for SF. Eq. (20) for SF proposed by Takaki et al.[12] underestimated δ in the transition region between laminar and turbulent flows.

Many δ correlations for the free falling films have been proposed as the form of $\delta/L_v = a\, Re_L{}^n$, where n = 1/3 for the laminar flow.[21] Several n values have been proposed for the turbulent flow and they are n = 0.6 and 2/3,[1] n = 2/3,[23] n = 8/15,[24] and n = 1/2 [19] depending on the database. In this study, we redetermined α by using Eq. (2), Eq. (13), and $(dP/dz)^*$ and CCFL data by Bharathan et al.[3] and by Ilyukhin et al.[9] We derived δ correlations for the transition and turbulent regions by using our α data and the redetermined α. We used the form of $\delta/L_v = a\, Re_L{}^n$, and n = 1/2 for the transition region and n = 2/3 for the turbulent region, and we obtained the a value as the average in the ranges of 1000 < Re_L < 3000 and Re_L > 3000 for the transition and turbulent regions, respectively. The derived correlation was expressed by:

$$\frac{\delta}{L_v} = \max\left\{ \left(\frac{3Re_L}{4}\right)^{1/3} \ ,\ 0.32 Re_L{}^{1/2} \ ,\ 0.076 Re_L{}^{2/3} \right\}. \tag{21}$$

Figure 8 compares Eq. (21) with data for (a) δ/L_v and (b) α. In the computation of $(1-\alpha)$ with Eq. (2), the maximum difference between Eqs. (11) and (13) for f_w was 0.0045 at Re_L = 1300 and its effect on δ was 12 %. The δ value by Eq. (21) was 133 % of the δ value by Eq. (18) at Re_L = 10000. The uncertainty of $\pm$0.0062 for the void fraction included 95 % of the data points. This showed that Eq. (21) gave good agreement with α data.

III.B. Interfacial Friction Factor

To evaluate f_i, accurate measurement of dP/dz is needed, because f_i is in proportion to $-dP/dz$ as expressed by Eq. (1) and $-dP/dz$ for SF is small as shown in Fig. 4. On the other hand, the effect of uncertainty in the α evaluation is relatively small because α is relatively large.

Figure 9 shows f_i evaluated from dP/dz data reported by Bharathan et al.[3] In the region of $J_G^* > 0.5$ (where $J_L = 0$), flooding occurred near the rounded bottom end, and $-dP/dz$ and $(1-\alpha)$ increased. In the region of SF (where $J_G^* < 0.5$), $-dP/dz$ was small and its change with increasing J_G was small. This made uncertainty for f_i large. The f_i values reported by Bharathan et al.[3] were large at small J_G^* as shown in Fig. 9, because they neglected the $J_L/(1-\alpha)$ term in Eq. (1) assuming $|J_L|/(1-\alpha) << J_G/\alpha$. Figure 9 showed that the f_i values computed with Eqs. (1), (2) and (13) and dP/dz data (where J_L^* measured for a given J_G^* was used) agreed well with the f_i values obtained from dP/dz and δ data and Eq. (1). This was due to the small effect of the α value on f_i.

Figure 10 shows f_i evaluated from dP/dz data reported by Ilyukhin et al.[9] Dispersion of dP/dz data reported by Ilyukhin et al.[9] was large compared with data reported by Shimamura et al.[7] This large dispersion led to the large dispersion for the f_i value in Fig. 10, which was computed with Eqs. (1), (2) and (13) and dP/dz data. The f_i value by Shimamura et al.[7] was obtained from dP/dz and α data and Eq. (1).

For RF, Sano et al.[17] proposed Eq. (16) as a function of K_G^*. The constant A and exponent B for $f_i = A\, K_G^{*B}$ were obtained for each experiment by using the least square method, and A and B were expressed by functions of D^* and the density ratio of gas and liquid phases ρ_G/ρ_L. As a result, we derived the following f_i correlation.

$$f_i = A\, K_G^{*B},$$

$$A = \left(\frac{9.0}{10^5}\right)\left(\frac{\rho_L}{\rho_G}\right)^{0.60} D^*,$$

$$B = \frac{-25\left(\rho_G / \rho_L\right)^{0.25}}{D^{*\,0.50}} \quad \text{for } 7.8 \leq D^* \leq 18.6. \tag{22}$$

Figure 11 shows effects of (a) diameters and (b) fluid properties on f_i for SF as a function of δ/L, which is used in Eq. (15). From A and B for $f_i = A\ (\delta/L)^B$ shown in Fig. 11, A and B were expressed by functions of D^* and ρ_G/ρ_L, and we derived the following f_i correlation.

$$f_i = A\left(\frac{\delta}{L}\right)^{\mathrm{B}},$$

$$A = \frac{260\left(\rho_L / \rho_G\right)^{0.35}}{D^{*2.9}},$$

$$B = \frac{11.4}{D^{*0.73}} \quad \text{for } 7.8 \leq D^* \leq 18.6. \tag{23}$$

Figure 12 (a) and (b) compare $f_{i,c}$ values computed with the derived correlations, Eqs. (22) and (23), with the measured $f_{i,m}$, respectively. In Fig. 12 (a), Eq. (22) underestimated f_i for D = 40 mm, but overestimated f_i for D = 50.8 mm. On the other hand, in Fig. 12 (b), Eq. (23) gave good agreement with $f_{i,m}$. Figure 12 showed that Eq. (23) was better than Eq. (22) for a f_i correlation.

III.C. Drift-Flux Parameters

In Eqs. (1) and (2), J_G^* is generally a given condition, J_L^* is obtained from a CCFL correlation, and α and $(dP/dz)^*$ are solved by using correlations for f_w and f_i. In some accident analysis codes, the drift-flux model proposed by Zuber and Findlay[13] is used instead of the f_i correlation. The general expression of the one-dimensional drift-flux model is:

$$\frac{\langle J_G \rangle}{\langle \alpha \rangle} = C_0 \langle J \rangle + V_{gj}, \tag{24}$$

$$<J> = <J_G + J_L> , \quad (25)$$

where $<J_G>$ is the area-averaged superficial gas velocity, $<J>$ is the area-averaged mixture volumetric flux, $<\alpha>$ is the area-averaged void fraction, C_0 is the distribution parameter, and V_{gj} is the drift velocity.

Figure 13 shows the drift-flux plots for SF with working fluids of (a) air-water and (b) steam-water. $C_0 = 1$ was a good approximation for all cases due to the reason of annular flows. Figure 14 shows the dimensionless drift velocity V_{gj}^* ($= V_{gj} /[\sigma \cdot g \cdot (\rho_L - \rho_G)/\rho_L^2]^{1/4}$) with the approximation of $C_0 = 1$ for SF with working fluids of (a) air-water and (b) steam-water. V_{gj}^* was about 2.0 for S/R in the mid gas velocity of $K_G^* = 0.5\text{-}1$ and V_{gj}^* decreased with increasing K_G^*. V_{gj}^* for S/S was smaller than V_{gj}^* for S/R. V_{gj}^* for high pressure steam-water was 0.7-1.1 and was smaller than V_{gj}^* for air-water. From Fig. 14, the correlations for the drift-flux parameters (C_0 and V_{gj}) were expressed by:

$$C_0 = 1, \quad (26)$$

$$V_{gj}^* = \min\left[\frac{\max\left\{0.014\left(\rho_L / \rho_G\right)^{0.74}, 0.76\right\}}{K_G^{*0.37}}, 2.0\right] \quad \text{for } 7.8 \le D^* \le 18.6, \quad (27)$$

$$V_{gj}^* = \frac{V_{gj}}{\left\{\sigma \cdot g \cdot \left(\rho_L - \rho_G\right) / \rho_L^2\right\}^{1/4}}, \quad (28)$$

where the density ratio of gas and liquid phases ρ_G/ρ_L was used. The restricted values of 0.76 and 2.0 were for high pressure and small K_G^*, respectively. When the viscosity ratio of gas and liquid phases μ_G/μ_L was used, the correlation for V_{gj}^* with $C_0 = 1$ was expressed by:

$$V_{gj}^* = \min\left[\frac{\max\left\{0.26\left(\mu_L / \mu_G\right)^{0.50}, 0.76\right\}}{K_G^{*0.37}}, 2.0\right] \quad \text{for } 7.8 \le D^* \le 18.6. \quad (29)$$

Figure 15 compares α_c computed with Eqs. (24), (26) and (27) or (29) with the measured α_m. The uncertainty, which included 95 % of the data points, was ±0.015 for (a) Eqs. (24), (26) and (27) and ±0.013 for (b) Eqs. (24), (26) and (29). The difference between α_c and α_m was relatively large in comparison with ±0.0062 for Eq. (21) shown in Fig. 8 (b).

IV. EFFECTS OF DIAMETER AND FLUID PROPERTIES

Our target for the derived correlations was to apply them to an accident analysis for a small-break loss-of-coolant accident in a PWR, where the maximum vertical pipe is about 0.3 m in the diameter for the pressurizer surge line and the highest pressure for two-phase flows in the primary loop may be mainly up to 7 MPa. The maximum value for the dimensionless diameter is $D^* = D/L = 187$ at 7 MPa for $D = 0.30$ m.

Eq. (7) for CCFL characteristics was derived from data of $D^* \leq 94$. Existing CCFL data for vertical pipes show that the CCFL constant C_K with the Kutateladze parameters like Eq. (7) approaches a constant value with increasing D^*.[5,11,25,26] Therefore, Eq. (7) for vertical pipes may be applied up to $D^* = 187$. Eq. (13) for f_w may be applied up to $D^* = 187$ because it is basically based on the correlation for single-phase flows.

IV.A. Correlation for Liquid Film Thickness

Applicability of Eq. (21) for δ to large D^* was not clear, hence we evaluated its rationality to large D^*. Figure 16 shows δ values calculated by Eq. (21) for effects of (a) D and (b) P (i.e. fluid properties). There are no data to confirm validity of the calculated values, but they did not show unreasonable trends.

IV.B. Correlation for Interfacial Friction Factor

It seems that Eqs. (7) for CCFL, (13) for f_w and (21) for δ may be applied up to $D^* = 187$ ($D = 0.3$ m and $P = 7$MPa). We can calculate dP/dz and f_i by using the momentum equations of Eqs. (1) and (2) and the correlations of Eqs. (7), (13) and (21). Figure 17 shows the computed f_i from Eqs. (1) and (2) and Eqs. (7), (13) and (21). f_i increases with increasing D due to the increase in δ shown in Fig. 16. J_G for a given J_G^* or K_G^* decreases with increasing P mainly due to the increase in ρ_G. There are no data to confirm validity of the calculated values, but they did not show unreasonable trends.

Eq. (23) for f_i gave irrationally small f_i for large D^* due to the term of $D^{*-2.9}$ for the coefficient A. Eq. (22) for f_i gave small change of f_i for changing K_G^* due to the term of $D^{*-0.50}$ for the exponent B in comparison with f_i calculated by Eqs. (1), (2), (7), (13) and (21). $f_i = A \exp(B K_G^*)$ was better than $f_i = A K_G^{*B}$ in Eq. (22), hence A and B for $f_i = A \exp(B K_G^*)$ were obtained for f_i shown in Fig. 17 by using the least square method. A and B were expressed by functions of D^* and ρ_G/ρ_L. As a result, we derived the following f_i correlation.

$$f_i = A \exp(B K_G^*),$$

$$A = \left(\frac{3.76}{10^4}\right)\left(\frac{\rho_L}{\rho_G}\right)^{0.76} D^* \quad ,$$

$$B = -0.654\left(\frac{\rho_L}{\rho_G}\right)^{0.11} D^{*0.16} \quad \text{for } 15 \le D^* \le 187. \qquad (30)$$

Figure 18 shows $f_{i,corr}$ calculated by Eq. (30) comparing with $f_{i,cal}$ shown in Fig. 17. $f_{i,corr}$ and $f_{i,cal}$ agreed well for air-water conditions except small f_i (< 0.01). Wallis[1] suggested f_i > 0.005 and the f_i value in the region of f_i < 0.01 is not important. The difference between $f_{i,corr}$ and $f_{i,cal}$ became large at high pressures. Eq. (22) or (23) agreed better for the f_i data with relatively small diameters than Eq. (30).

IV.C. Correlation for Drift-Flux Parameters

From Eqs. (24)-(26), $\langle\alpha\rangle = \langle J_G\rangle/\{\langle J_G+J_L\rangle + V_{gj}\}$. Eq. (27) or (29) cannot be applied to large D and high P because of $\alpha > 1.0$ due to $\{\langle J_G+J_L\rangle + V_{gj}\} < J_G$ for small J_G

(i.e. large $|J_L|$). α can be obtained from Eq. (17) and δ by Eq. (21). The correlation for the drift velocity V_{gj} was obtained from $C_0 = 1$, δ in Fig. 8 (a) by data, and Fig. 16 by Eq. (21) as:

$$V_{gj}^* = \max(A, B),\ 0 \le V_{gj}^* \le 2.2 \text{ for } 7.8 \le D^* \le 187$$

$$A = 1.0\frac{(\rho_L/\rho_G)^{0.24}}{D^{*0.20}} - 0.315\left(\frac{\rho_L}{\rho_G}\right)^{0.317} K_G^*,$$

$$B = 0.76\frac{(\rho_L/\rho_G)^{0.15}}{D^{*0.20}} - 0.515\left(\frac{\rho_L}{\rho_G}\right)^{0.032} \ln\left(K_G^*\right). \quad (31)$$

$V_{gj}^* = 0$ and 2.2 in $0 \le V_{gj}^* \le 2.2$ show the lower and upper limits of V_{gj}^*, respectively. The first term A and second term B are for low P and high P, respectively. Figure 19 shows the relationship between α_{corr} by Eqs. (24), (26) and (31) and α_{cal} by Eq. (21) (i.e. δ shown in Fig. 16). α_{corr} was lower than α_{cal} at low α for medium D. Eq. (27) or (29) agreed better for the α data with relatively small diameters than Eq. (31). It was difficult to derive a V_{gj}^* correlation for wide range of conditions, and it is recommended to obtain a V_{gj}^* correlation for a given D.

V. CONCLUSIONS

In this study, we compared the data by Goda et al.[6] for $D = 40$ mm with the rounded top and square bottom ends (R/S) and the data by Takaki et al.[8] for $D = 40$ mm with the square top and rounded bottom ends (S/R) to evaluate features of flow characteristics for the rough film (RF) due to flooding at the bottom end and the smooth film (SF) due to flooding at the top end. We obtained the liquid film δ (or void fraction α) and interfacial friction factor f_i by using the correlation of the wall friction factor f_w proposed by Takaki et al.[8] and dP/dz data reported by Bharathan et al.[3] and Ilyukhin et al.,[9] and we derived empirical correlations for δ and f_i for SF.

(1) For SF in the region of low J_G, $(1-\alpha)$ and f_i under flooding conditions were larger for R/S than they were for S/R due to large J_L for R/S.

(2) δ for SF was well expressed by a function of the liquid Reynolds number Re_L as $\delta \propto Re_L^{1/3}$ (i.e. Nusselt equation), $Re_L^{1/2}$ and $Re_L^{2/3}$ for the laminar flow, transition, and turbulent flow, respectively. The uncertainty of the correlation proposed for δ, Eq. (21), which included 95 % of the data points, was ±0.0062 for α = 0.87-0.98.

(3) δ/L (where L is Laplace length) was better than the gas Kutateladze parameter K_G^* to express f_i for SF, and Eq. (23) was derived as a function of δ/L, the dimensionless diameter D^*, and the density ratio of gas and liquid phases ρ_G/ρ_L. On the other hand, Eq. (30) (which was a function of K_G^*, D^*, and ρ_G/ρ_L) was recommended for large D and high pressure P.

(4) The drift-flux parameters (C_0 and V_{gj}) for SF were evaluated. The distribution parameter was C_0 = 1 due to the annular flow, and a correlation for the dimensionless drift velocity V_{gj}^* was derived as a function of K_G^* and the viscosity ratio of gas and liquid phases μ_G/μ_L. The uncertainty (which included 95 % of the data points) was ±0.013 for α computed with the drift-flux Eqs. (24), (26) and (29), which could not be applied to large D and high P. Eq. (31) was proposed for V_{gj}^* at large D and high P.

NOMENCLATURE

C	CCFL constant (-)
C_0	distribution parameter (-)
D	pipe diameter (m)
D^*	dimensionless pipe diameter (-)
f_i	interfacial friction factor (-)

f_w wall friction factor (-)

g gravitational acceleration (m/s^2)

h water level in the upper tank (m)

J superficial velocity (m/s)

J^* Wallis parameter (-)

K^* Kutateladze parameter (-)

L Laplace length (m)

L_v length defined by Eq. (14) (m)

m slope of CCFL characteristics (-)

P pressure (Pa)

Re Reynolds number (-)

V_{gj} drift velocity (m/s)

V_{gj}^* dimensionless drift velocity (-)

W_L liquid flow rate limited by flooding (m^3/s)

z axial coordinate (m)

Greek

α void fraction (-)

δ liquid film thickness (m)

μ viscosity (Pa s)

ν kinematic viscosity (m^2/s)

ρ density (kg/m^3)

σ surface tension (N/m)

Subscript

B bottom

c computed

G	gas phase
i	G or L
L	liquid phase
m	measured
T	top

Superscript

*	dimensionless form

References

1. G. B. WALLIS, *One-Dimensional Two-Phase Flow*, pp. 336-345, McGraw Hill, New York (1969).
2. S. G. BANKOFF, and S. C. LEE, "A Critical Review of the Flooding Literature," NUREG/CR-3060, U.S. Nuclear Regulatory Commission (1983).
3. D. BHARATHAN, G. B. WALLIS, and H. J. RICHTER, "Air-Water Countercurrent Annular Flow in Vertical Tubes," EPRI NP-786, Electric Power Research Institute (1978).
4. D. BHARATHAN, G. B. WALLIS, and H. J. RICHTER, "Air-Water Countercurrent Annular Flow," EPRI NP-1165, Electric Power Research Institute (1979).
5. D. BHARATHAN, and G. B. WALLIS, "Air-Water Countercurrent Annular Flow," *Int. J. Multiphase Flow*, **9**, *4*, 349 (1983); https://doi.org/10.1016/0301-9322(83) 90093-9.
6. R. GODA et al., "Experimental Study on Interfacial and Wall Friction Factors under Counter-Current Flow Limitation in Vertical Pipes with Sharp-Edged Lower Ends," *Nucl. Eng. Des.*, **353**. 110223 (2019); https://doi.org/10.1016/j.nucengdes.2019. 110223.

7. T. SHIMAMURA et al., “Interfacial and Wall Frictions under Flooding Conditions in a Vertical Pipe with the Sharp-Edged Upper End,” *Proc. of Jpn. Symposium on Multiphase Flow 2018*, Sendai, Japan, August 8-10, 2018, D212 (in Japanese).
8. T. TAKAKI et al., “Flow Characteristics in Vertical Circular Pipes with the Square Top End under Flooding Conditions,” *Nucl. Eng. Des.*, **371**, 110951 (2021); https://doi.org/10.1016/j.nucengdes.2020.110951.
9. Yu. N. ILYUKHIN et al., “Hydrodynamic Characteristics of Annular Counter Flows in Vertical Channels,” *Teplofiz. Vys. Temp*., **26**, *5*, 923 (1988) (in Russian).
10. T. DOI et al., “Countercurrent Flow Limitation at the Junction Between the Surge Line and the Pressurizer of a PWR,” *Sci. Technol. Nucl. Installations*, **2012**, 754724 (2012); https://doi.org/10.1155/2012/754724.
11. M. MURASE et al., “Effects of Diameters on Countercurrent Flow Limitation at a Square Top End in Vertical Pipes,” *Sci. Technol. Nucl. Installations*, **2018**, 1426718, (2018); https://doi.org/10.1155/2018/1426718.
12. T. TAKAKI et al., “Liquid Film Thickness in Vertical Circular Pipes under Flooding Conditions at the Top End,” *Nucl. Technol.*, **206**, *3*, 389 (2020); https://doi.org/ 10.1080/00295450.2019.1656521.
13. N. ZUBER, and J. FINDLAY, “Average Volumetric Concentration in Two-Phase Flow Systems,” *J. Heat Transfer*, **87**, 453 (1965).
14. T. KUSUNOKI et al., “Effects of Fluid Properties on CCFL Characteristics at a Vertical Pipe Lower End,” *J. Nucl. Sci. Technol.*, **52**, 887 (2015); https://doi.org/ 10.1080/00223131.2014.990533.
15. T. KUSUNOKI et al., “Condensation Experiments for Counter-Current Flow Limitation in an Inverted U-Tube,” *J. Nucl. Sci. Technol.*, **53**, 486 (2016); https:// doi.org/10.1080/00223131.2015.1057253.

16. Y. SUDO, “Limitation of Falling Water in Countercurrent Two-Phase Flow in Vertical Circular Tubes,” *Trans. of the JSME*, **60**, 2566 (1994) (in Japanese); https://doi.org/10.1299/kikaib.60.2566.

17. N. SANO et al., “Interfacial Friction Factors in Vertical Circular Pipes under Flooding Conditions at the Bottom End,” *Jpn. J. Multiphase Flow*, **34**, 82 (2020) (in Japanese); https://doi.org/10.3811/jjmf.2020.029.

18. S. KAMEI et al., “Hold-Up in a Wetted Wall Tower,” *Kagaku-kogaku*, **18**, 545 (1954) (in Japanese).

19. K. FEIND, “Shrömungsuntersuchungen bei Gegensttom von Rieselfilmen und Gas in Lotrechten Rohren,” *VDI-Forschungsheft*, **481** (1960) (in German).

20. G. F. HEWITT, and G. B. WALLIS, “Flooding and Associated Phenomena in Falling Film Flow in a Tube,” AERE-R4022, Atomic Energy Research Establishment (1963).

21. W. NUSSELT, “Die Oberflachenkondensation des Wasserdampfes,” *Vereines Deutscher Ingenieure*, **60**, 541 (1916) (in German).

22. H. IMURA et al., “Flooding Velocity in a Counter-Current Annular Two-Phase Flow,” *Chemical Eng. Sci.*, **32**, 79 (1977); https://doi.org/10.1016/0009-2509(77)80199-1.

23. W. BRÖTZ, “Über die Vorausberechunug der Absorptionsgeschwindigkeit von Gasen in Strömenden Flüssigkeitsschichten,” *Chemie. Ing. Techn*., **26**, 470 (1954) (in German).

24. H. BRAUER, “Strömungsuntersuchungen und Wärmeubergang bei Rieselfilmen,” B22, VDI Forscungsheft, 457 (1956) (in German).

25. G. B. WALLIS, and S. MAKKENCHERY, “The Hanging Film Phenomenon in Vertical Annular Two-Phase Flow,” *J. Fluids Eng*. **96**, *3*, 297 (1974); https://doi.org/10.1115/ 1.3447155.

26. G. B. WALIS, and J. T. KUO, “The Behavior of Gas-Liquid Interfaces in Vertical Tubes,” *Int. J. Multiphase Flow*, **2**, 521 (1976); https://doi.org/10.1016/0301-9322(76) 90013-6.

TABLE I

Experimental Conditions

Reference	D (mm)	Top/Bottom	Fluids	P (MPa)	h (m)	Data
Goda et al.[6]	20, 40	R/S	A-W	0.1	0.1	α, dP/dz
Shimamura et al.[7]	20	S/R	A-W	0.1	0.1	α, dP/dz
Takaki et al.[8]	40	S/R	A-W	0.1	0.1	α, dP/dz
Bharathan et al.[3]	50.8	S/S, S/R, R/S	A-W	0.1	> 0.1	δ, dP/dz
Ilyukhin et al.[9]	20	S/S	S-W	0.6-4.1	(high)	dP/dz

Top/Bottom: R, rounded; S, square. Fluids: A, air; S, steam; W, water.
D, diameter; h, water level in the upper tank; P, pressure; dP/dz, pressure gradient; α, void fraction; δ, liquid film thickness

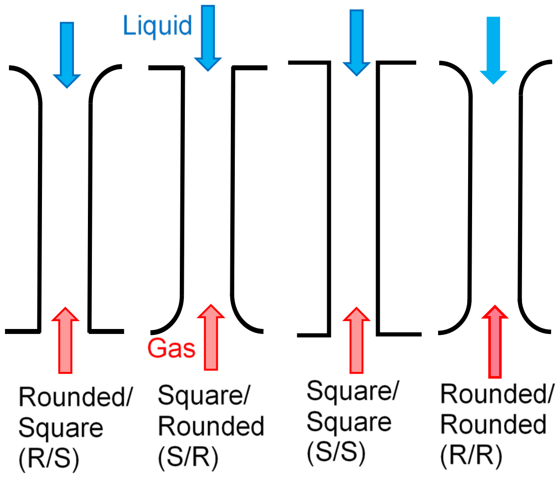

(a) Top and bottom end shapes

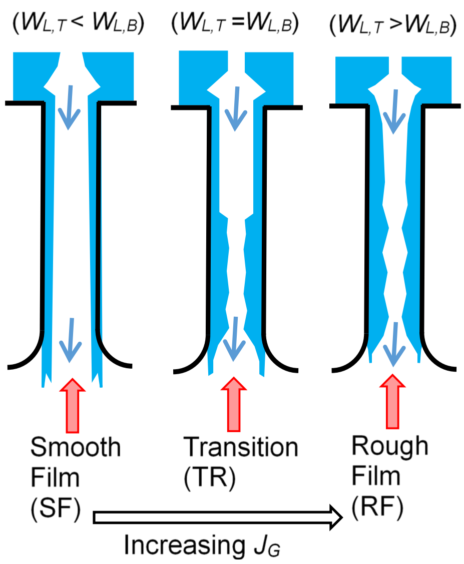

(b) Flow patterns under flooding conditions
(W_L, liquid flow rate limited by flooding; B, bottom end; T, top end)
Fig. 1. Illustrations for top and bottom end shapes and flow patterns.

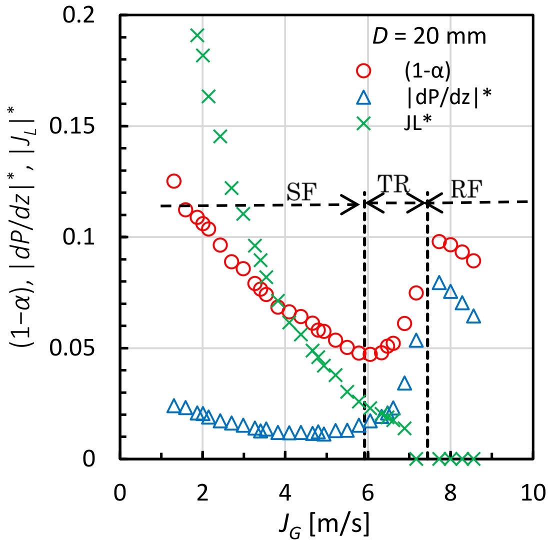

(a) Flow characteristics

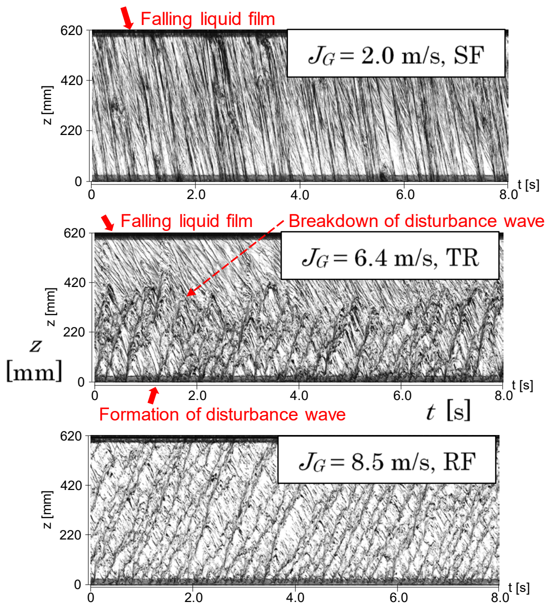

(b) Time-strip images

Fig. 2. Features of flow characteristics and flow patterns in a vertical pipe with the square top and rounded bottom ends under flooding conditions reported by Shimamura et al.[7] (SF, smooth film; TR, transition; RF, rough film).

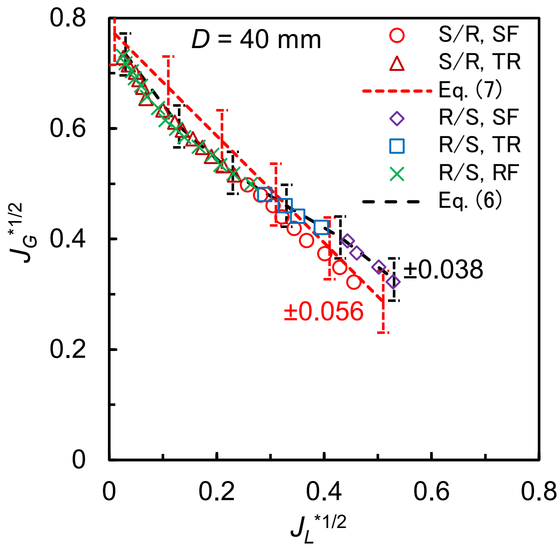

Fig. 3. CCFL characteristics (S/R and R/S, see Table I; SF, smooth film; TR, transition, RF, rough film).

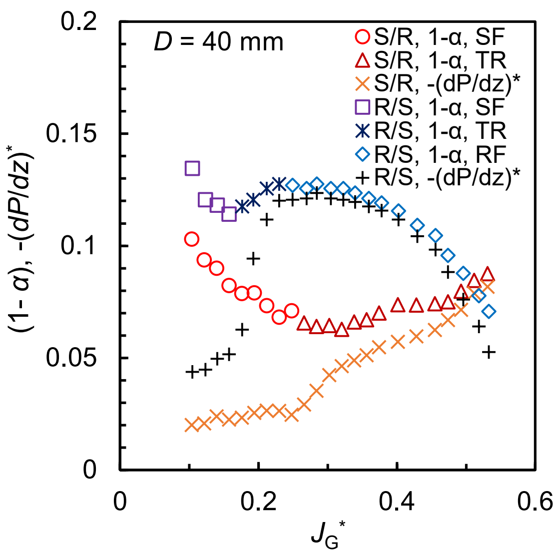

Fig. 4. Liquid volume fraction (1–α) and dimensionless pressure gradient $(dP/dz)^*$.

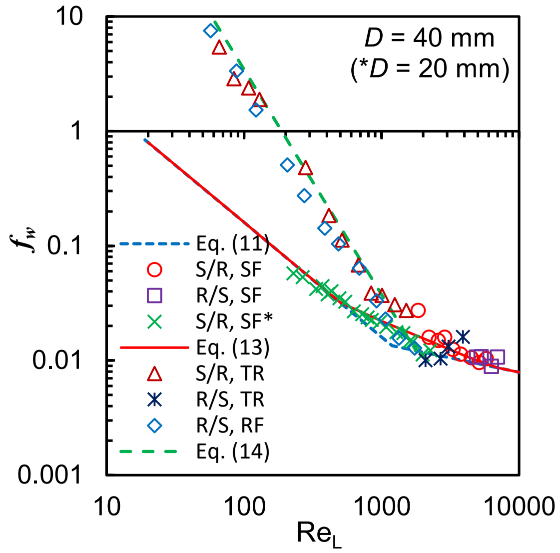

Fig. 5. Wall friction factor f_w (*Shimamura et al.[7]).

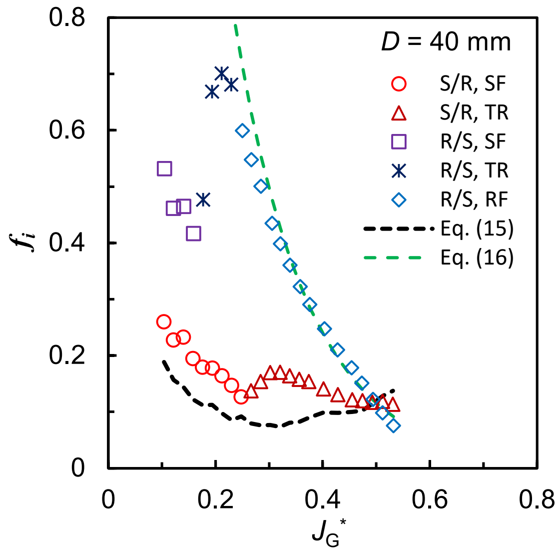

Fig. 6. Interfacial friction factor f_i.

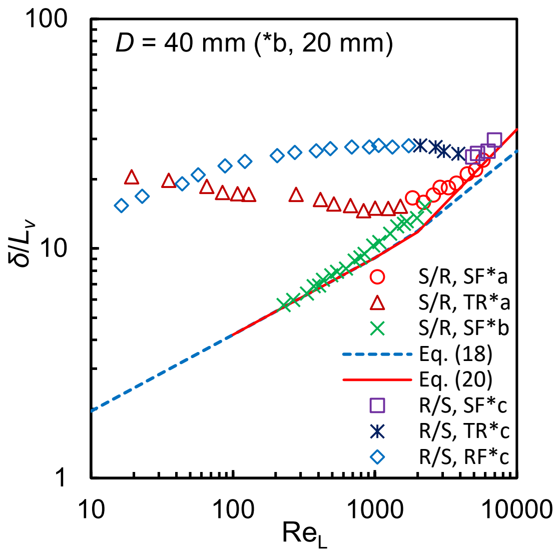

Fig. 7. Dimensionless liquid film thickness δ/L_v (*a, Takaki et al.[8]; *b, Shimamura et al.[7], *c, Goda et al.[6]).

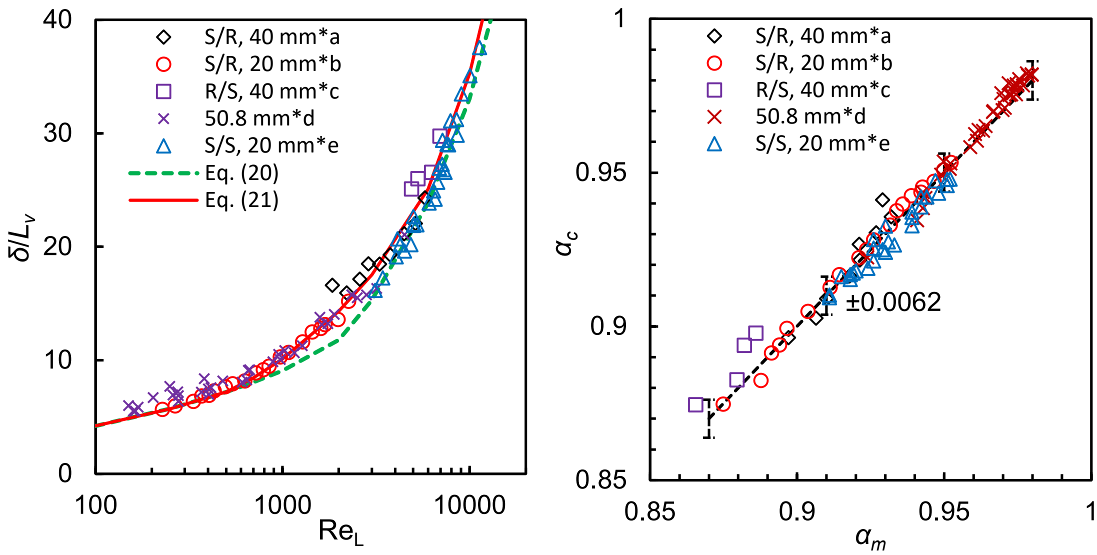

(a) Liquid film thickness (b) Void fraction

Fig. 8. Comparison of Eq. (21) with data for the liquid film thickness δ/L_v and void fraction α. α_c and α_m are α computed with Eq. (21) and α measured, respectively (*a, Takaki et al.[8]; *b, Shimamura et al.[7]; *c, Goda et al.[6]; *d, Bharathan et al.[3]; *e, Ilyukhin et al.[9]).

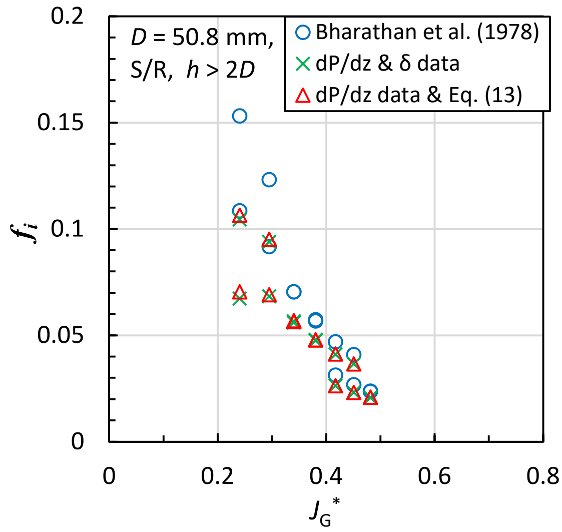

Fig. 9. Interfacial friction factor f_i obtained from data by Bharathan et al.[3]

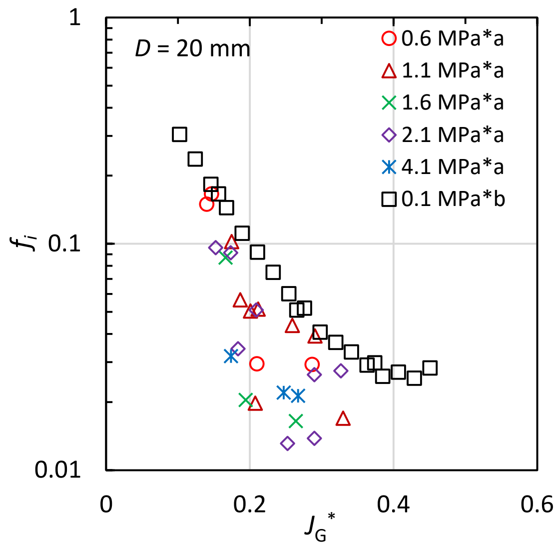

Fig. 10. Interfacial friction factor f_i obtained from data reported by Ilyukhin et al.[9] (*a, Ilyukhin et al.[9]; *b, Shimamura et al.[7]).

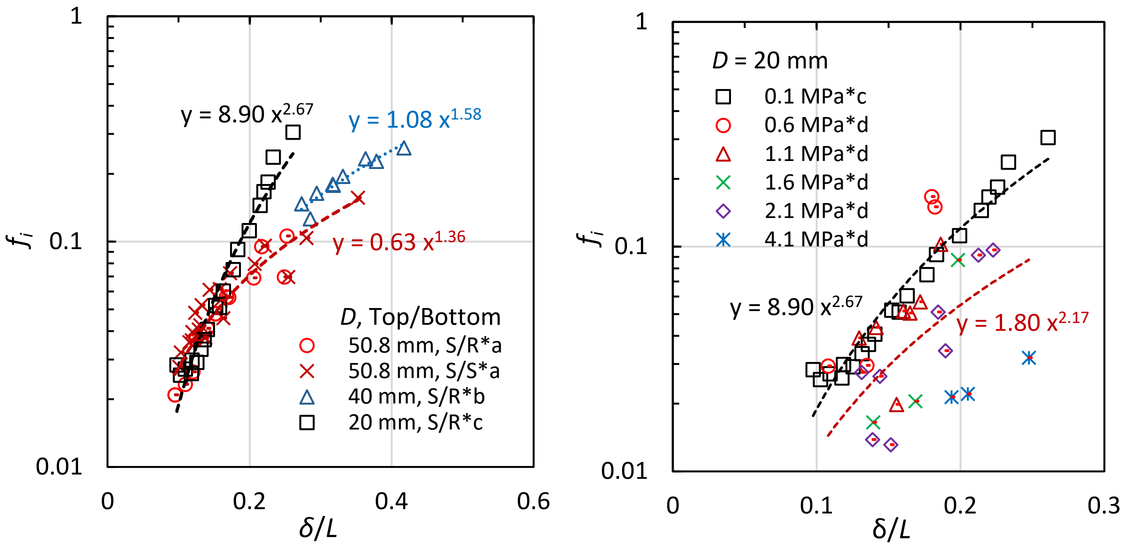

(a) Effects of diameters with air-water (b) Effects of fluid properties with $D = 20$ mm

Fig. 11. Effects of diameters and fluid properties on f_i as a function of δ/L (*a, Bharathan et al.[3]; *b, Takaki et al.[8]; *c, Shimamura et al.[7]; *d, Ilyukhin et al.[9]; S/R and S/S, see Table I; x =δ/L; y = f_i).

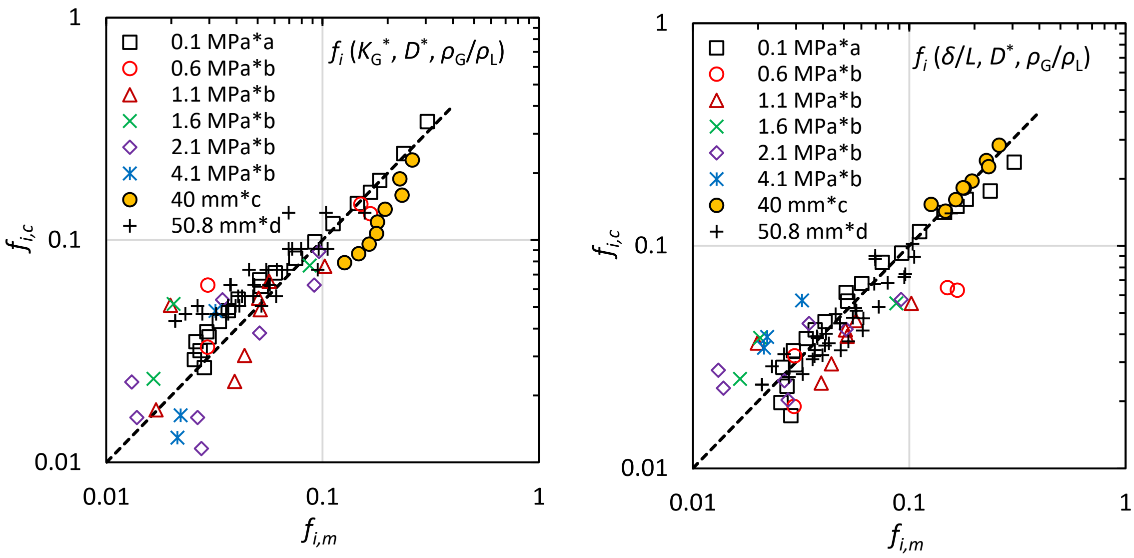

(a) $f_{i,c}$ computed with Eq. (22) (b) $f_{i,c}$ computed with Eq. (23)

Fig. 12. Comparison of $f_{i,c}$ values computed with the derived correlations, Eqs. (22) and (23), with the measured $f_{i,m}$ (*a, Shimamura et al.[7]; *b, Ilyukhin et al.[9]; c*, Takaki et al.[8]; *d, Bharathan et al.[3]; *a and *b, $D = 20$ mm).

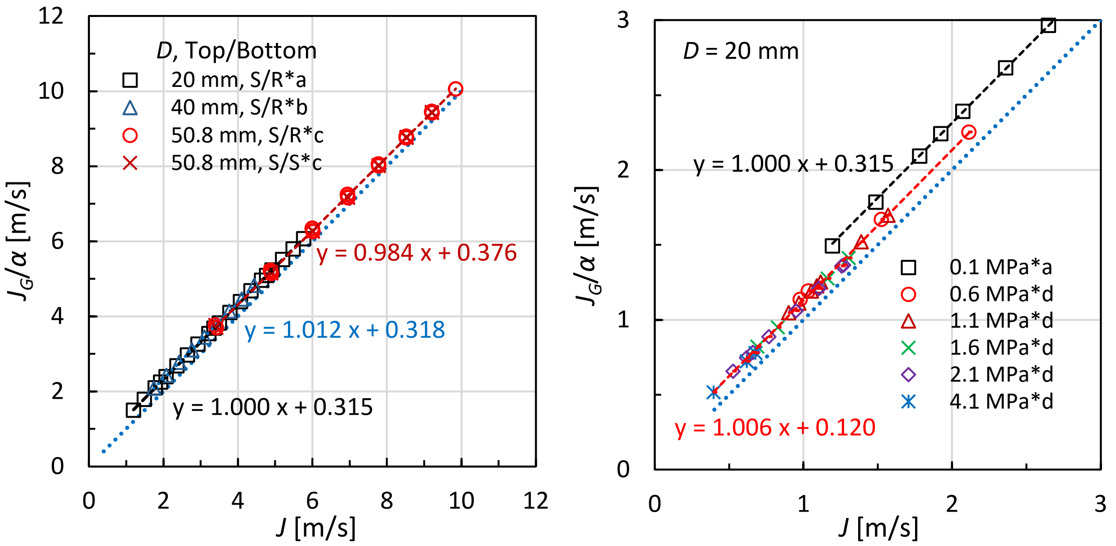

(a) Air-water conditions (b) D = 20 mm (effects of fluid properties)

Fig. 13. Drift-flux plots for the SF (*a, Shimamura et al.[7]; *b, Takaki et al.[8]; *c, Bharathan et al.[3]; *d, Ilyukhin et al.[9]; x = J; y = J_G/α).

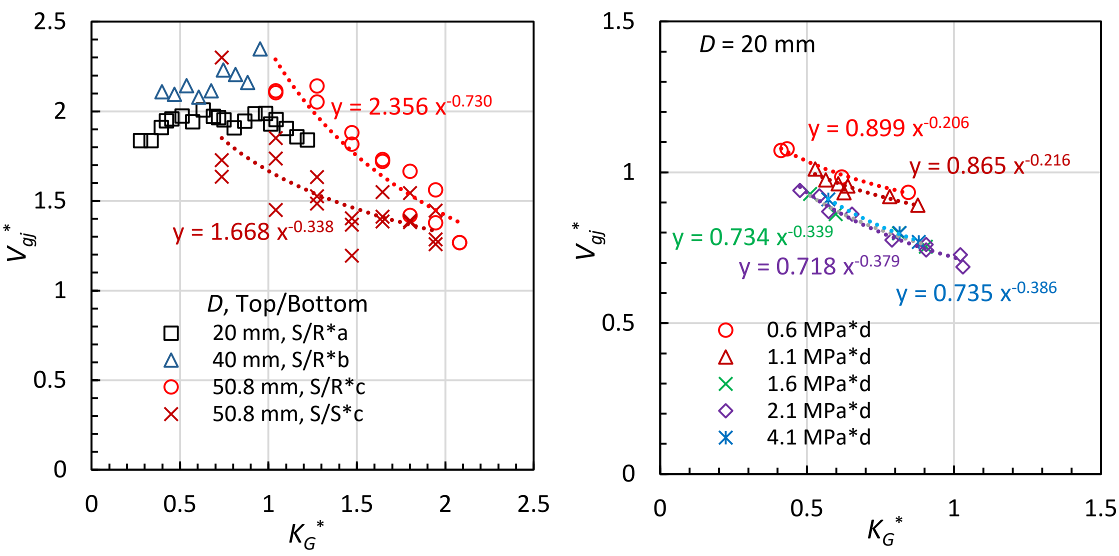

(a) Air-water conditions (b) Steam-water conditions (D = 20 mm)

Fig. 14. Dimensionless drift velocity V_{gj}^* with approximation of $C_0 = 1$ (*a, Shimamura et al.[7]; *b, Takaki et al.[8]; *c, Bharathan et al.[3]; *d, Ilyukhin et al.[9]; x = K_G^*; y = V_{gj}^*).

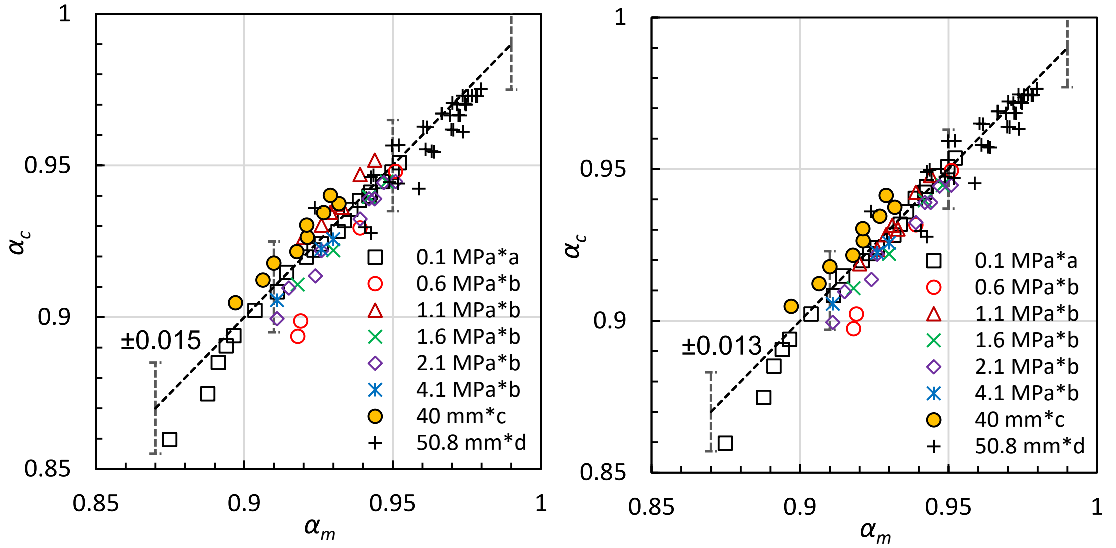

(a) Eqs. (24), (26) and (27) (b) Eqs. (24), (26) and (29)

Fig. 15. Comparison of α_c computed with the drift-flux correlation with the measured α_m (*a, Shimamura et al.[7]; *b, Ilyukhin et al.[9]; *c, Takaki et al.[8]; *d, Bharathan et al.[3]).

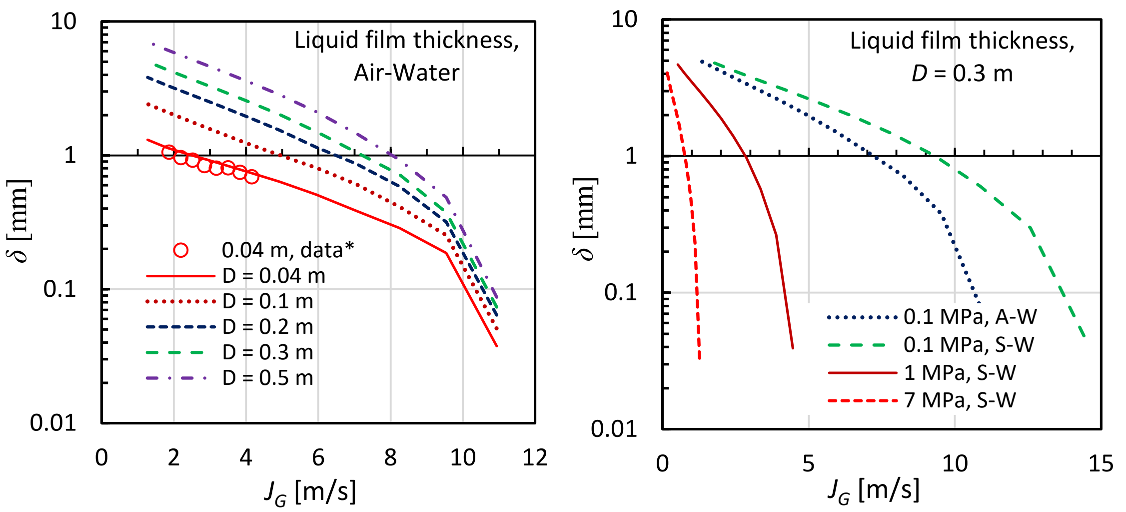

(a) Effects of diameters (air-water) (b) Effects of pressures (S-W: steam-water)

Fig. 16. Liquid film thickness calculated by Eq. (21) (*Takaki et al.[8]).

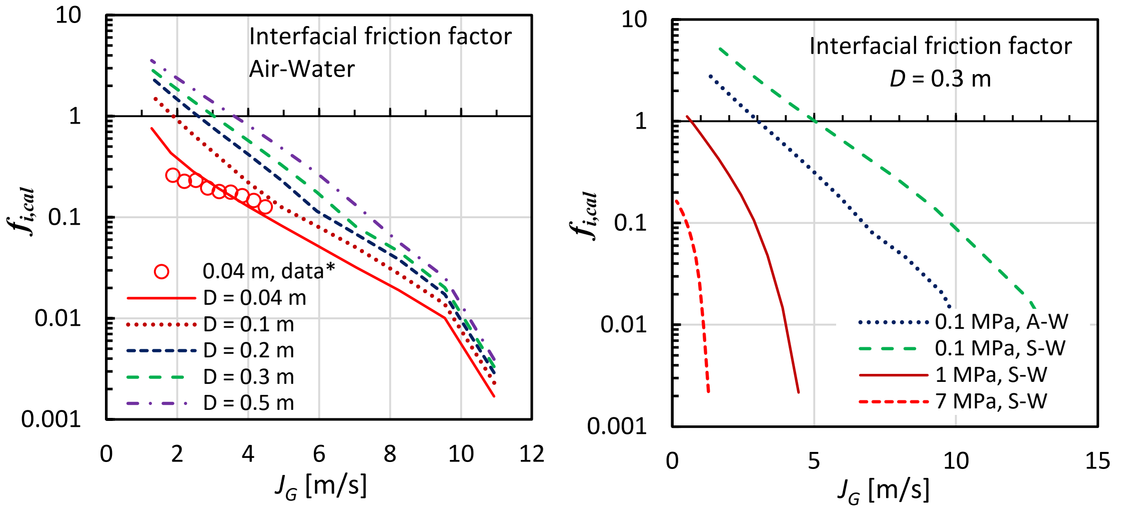

(a) Effects of diameters (air-water) (b) Effects of pressures (S-W: steam-water)

Fig. 17. Interfacial friction factor $f_{i,cal}$ calculated from Eqs. (1) and (2) and Eqs. (7), (13) and (21) (*Takaki et al.[8]).

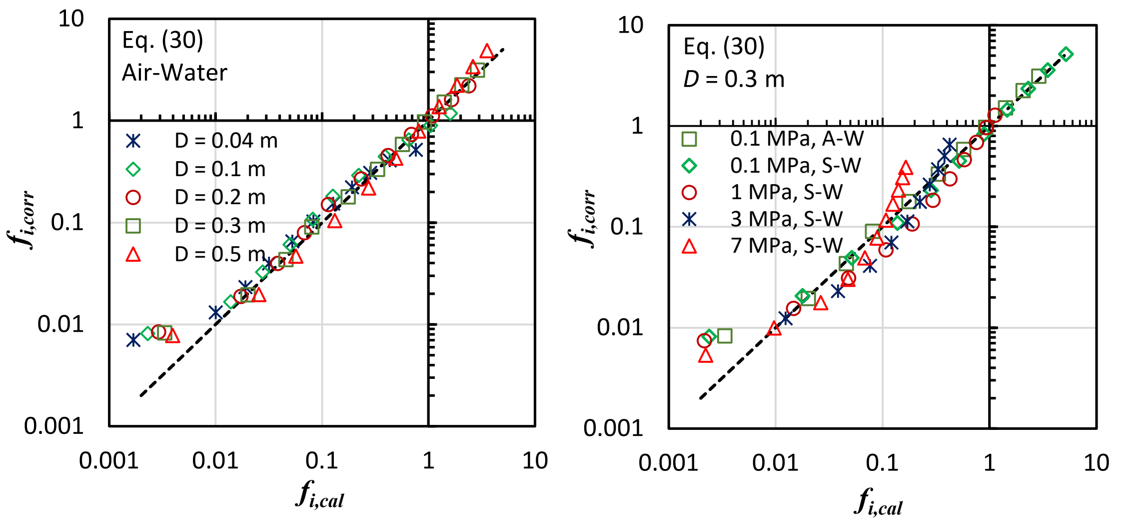

(a) Effects of diameters (air-water) (b) Effects of pressures (S-W: steam-water)

Fig. 18. Interfacial friction factor $f_{i,corr}$ calculated by the correlation of Eq. (30) for large D and high P.

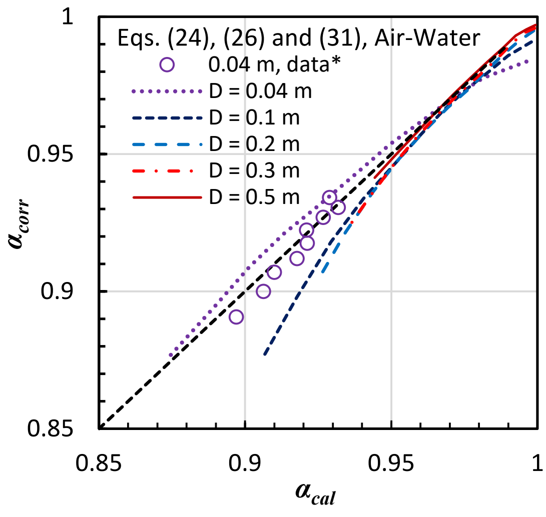

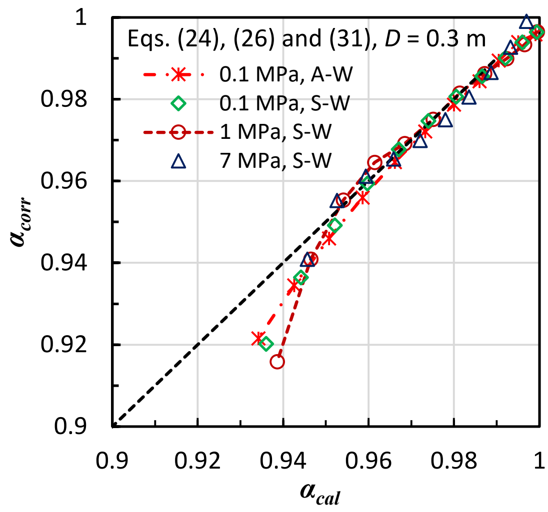

(a) Effects of diameters (air-water)   (b) Effects of pressures (S-W: steam-water)

Fig. 19. Relationship between α_{corr} by Eqs. (24), (26) and (31) and α_{cal} by Eq. (21) (*Takaki et al.[8]).